pHlameleons: A Family of FRET-Based Protein Sensors for Quantitative pH Imaging[†]

Alessandro Esposito,*[,‡] Matthias Gralle,[§] Maria Angela C. Dani, Dirk Lange, and Fred S. Wouters

Laboratory for Molecular and Cellular Systems, Department of Neuro- and Sensory Physiology, University Medicine Göttingen, Humboldtalee 23, 37073 Göttingen, Germany

Received May 20, 2008; Revised Manuscript Received October 6, 2008

ABSTRACT: Intracellular pH is an important indicator for cellular metabolism and pathogenesis. pH sensing in living cells has been achieved using a number of synthetic organic dyes and genetically expressible sensor proteins, even allowing the specific targeting of intracellular organelles. Ideally, a class of genetically encodeable sensors need to cover relevant cellular pH ranges. We present a FRET-based pH sensor platform, based on the pH modulation of YFP acceptor fluorophores in a fusion construct with ECFP. The concurrent loss of the overlap integral upon acidification results in a proportionally reduced FRET coupling. The readout of FRET over the sensitized YFP fluorescence lifetime yields a highly sensitive and robust pH measurement that is self-calibrated. The principle is demonstrated in the existing high-efficiency FRET fusion Cy11.5, and tunability of the platform design is demonstrated by genetic alteration of the pH sensitivity of the acceptor moiety.

A variety of organic (e.g., SNARF-1 and SNARF-4F) and genetically encoded (e.g., pHluorins and deGFPs)[1] biosensors are available for the detection of pH. Fluorophores like SNARF-1, SNARF-4F, and LysoSensors have been engineered to exhibit a strong spectral shift upon changes in pH with a pK_a (~4−7.5) in the physiological range (*1, 2*). Variants of fluorescent proteins have also been optimized to sense pH changes. Among these, pHluorin and deGFP4 allow quantitative ratiometric pH sensing by dual excitation and emission, respectively (*3, 4*). Genetically encoded biosensors are particularly interesting because they can be targeted to specific cell types and intracellular localizations, and because of their noninvasive mode of operation which guarantees minimal disturbance of cellular physiology. For instance, the ratiometric pHluorin was recently used for pH sensing in the digestive vacuole of *Plasmodium falciparum* (*5*), the mitochondrial alkaline pH indicator mtAlpHi permitted the measurement of pH variation in mitochondria (*6*), and the ecliptic property of YFP was used directly to detect pH variations in the Golgi (*7*).

The enhanced yellow fluorescent protein EYFP derived from enhanced GFP exhibits a strong dependence on pH with a pK_a of ~6.9 (*8*). The protonated chromophore of EYFP and many of its variants (here generically termed YFPs) are typically nonfluorescent because of a shift of the absorption peak to wavelengths lower than 450 nm (*9*), accompanied by a reduction in the molar extinction coefficient and quantum yield. On the other hand, the cyan fluorescent protein (ECFP) is far less sensitive to pH, exhibiting a pK_a of ~4.8 (*10*), and also partially retains its fluorescence when protonated.

pH-sensitive fluorophores allow the detection of pH variations; ratiometric biosensors offer the additional advantage of permitting a more quantitative and properly calibrated pH readout. In particular, ratiometric probes that shift their emission spectra are suitable for quantitative and rapid detection since they require only a single excitation wavelength and can be used with comparatively simple detection systems.

We therefore envisaged the possibility of enhancing a pH-induced emission spectral shift by using a genetically encoded pH biosensor based on the popular CFP−YFP tandem FRET sensor design. In our approach, ECFP fluorescence is quenched by efficient energy transfer to YFP and the differences in pH sensitivity of the two fluorescent proteins are exploited for the quantitative detection of pH changes. At higher pH, the emission spectrum of the YFP acceptor dominates when the probes are excited at the optimum for ECFP. At low pH, however, the shift in the

[†] F.S.W. is member of, and financed by, the "Molecular Microscopy" section and the Excellence Cluster 171 "Microscopy on the Nanometer Scale" of the DFG-funded (German Research Council) Center for Molecular Physiology of the Brain (CMPB). Additional financing from the German Federal Ministry for Education and Research (BMBF) for the project "FLI-Cam" in the Biophotonik III program is acknowledged. M.G. is funded by the Fritz Thyssen Foundation.

* To whom correspondence should be addressed. Phone: +44-1223-334193. Fax: +44-1223-334796. E-mail: aesposito@quantitative-microscopy.org.

[‡] Present address: Laser Analytics Group, Department of Chemical Engineering and Biotechnology, University of Cambridge, Pembroke Street, Cambridge CB2 3RA, U.K.

[§] Present address: Department of Evolutionary Genetics, Max Planck Institute for Evolutionary Anthropology, Deutscher Platz 6, 04103 Leipzig, Germany.

[1] Abbreviations: FRET, Förster resonance energy transfer; YFP, yellow fluorescent protein; ECFP, enhanced cyan fluorescent protein; SNARF, Seminaphthorhodafluors; deGFP, dual emission green fluorescent protein; mtAlpHi, mitochondrial alkaline pH indicator; GFP, green fluorescent protein; EYFP, enhanced yellow fluorescent protein; CHO, Chinese hamster ovary; FCS, fetal calf serum; DMEM, Dulbecco's modified Eagle's medium; P/S, penicillin and streptomycin; PC12, pheochromocytoma 12; AOBS, acoustoptical beam splitter; MCF-7, mammary adenocarcinoma cells; FLIM, fluorescence lifetime imaging microscopy; FD, frequency domain; SEM, standard error of the mean.

10.1021/bi8009482 CCC: $40.75
Published on Web 11/13/2008

YFP absorption spectrum diminishes the spectral overlap between ECFP and the protonated YFP, resulting in the dequenching of the donor ECFP by loss of FRET coupling.

Recently, a fusion construct of ECFP and YFP Venus called Cy11.5 was generated by deletion of eleven and five amino acids from the N- and C-termini of ECFP and Venus, respectively (*11*). The linker between the two proteins was optimized to allow the donor to transfer ~98% of the energy to the acceptor. Even though the causes for this exceptionally high FRET efficiency have not yet been completely elucidated, the resulting Cy11.5 possesses the useful property of being a long Stokes shift.

In this work, the pH sensitivity of Cy11.5 was first characterized. Furthermore, the truncated Venus was replaced with a similarly truncated EYFP and mutant EYFP-H148G (H148G for short). This generated three ratiometric biosensors with different pK_a values within the range of 5−7. The easy tunability of our sensor platform represents a unique advantage over earlier implementations as it allows both the selection of optimal sensitivity in desired pH ranges for different cellular pH responses, e.g., during lysosomal maturation or cytosolic acidification during high metabolic activity, and maintenance of high sensitivity in extended pH trajectories by the use of multiple sensors, e.g., during lysosomally induced nonapoptotic cell death. In analogy with its design templates, Cameleon (*12*) and Clomeleon (*13*), both fusion constructs of CFP and YFP for the ratiometric detection of calcium and chloride ions, respectively, we call this new family of pH biosensors pHlameleon. Furthermore, the measurement of the pH-modulated FRET efficiency by the sensitized acceptor emission fluorescence lifetime yields self-referenced sensors that do not require an additional calibration step. The proposed biosensor design, where changes in the absorption characteristics of an acceptor are read ratiometrically or by acceptor lifetime changes by virtue of energy transfer from a donor fluorophore, could also be used for the generation of other types of environmental biosensors.

EXPERIMENTAL PROCEDURES

Cloning. The Cy11.5 bacterial (pRSET) and mammalian (pcDNA3) plasmids were kindly provided by A. Miyawaki (Laboratory for Cell Function Dynamics, RIKEN Brain Science Institute, Wako City, Japan). The Cy11.5 cDNA is inserted between BamHI and EcoRI restriction sites and presents an XhoI site between the ECFP△11 and △5Venus coding sequences (*11*). pHlameleons were generated by replacing the N-terminally truncated Venus with similarly truncated EYFP and EYFP-H148G mutant proteins. The H148G mutation was generated by mutagenesis with the following forward (GAG TAC AAC TAC AAC AGC GGC AAC GTC TAT ATC ATG) and reverse (TAC AAC TAC AAC AGC GGC AAC GTC TAT ATC ATG GCC) primers.

Protein Purification. Chemically competent *Escherichia coli* BL21(DE3) cells (Invitrogen, Karlsruhe, Germany) were transformed with pRESET:pHlameleon; 500 mL liquid cultures (20 g of tryptone, 5 g of yeast, 0.5 g of NaCl, 10 mM $MgCl_2$, and 100 mg/mL ampicillin) were grown at 37 °C and 250 rpm at an optical density of ~0.6, induced with 1 mM IPTG (Roth, Karlsruhe, Germany) for ~6 h, and incubated at 16 °C overnight. Cells were harvested and lysed in BugBuster/Benzonase (VWR International-Calbiochem, Darmstadt, Germany). Cy11.5 and pHlameleon were purified using metal affinity chromatography on TALON resin columns (Ozyme-Clontech, Saint Quentin Yvelines Cedex, France) and dialyzed against phosphate-buffered saline (PBS) (Sigma, Munich, Germany) using Slide-A-Lyzer Dialysis Cassettes (10000 MWCO, 0.5−3 mL capacity by Pierce) according to the protocol provided by the supplier. One hundred microliters of cyanogen bromide-activated Sepharose beads (GE Healthcare-Amersham Biosciences, Freiburg, Germany) was activated in 1 mM HCl for 10−20 s and resuspended in 100 mM bicine buffer (pH ~8.5) after a short wash with the same buffer. One hundred microliters of protein (~5 mg/mL) was immediately added to the beads. The coupling reaction was quenched with 50 mM Tris-HCl (pH ~7.4), and beads were washed in PBS as soon as the buffer was cleared of fluorescent protein as inferred by visual inspection of the reaction mixture.

Buffers. The pH of the imaging medium and spectroscopy buffers was adjusted by the use of 25 mM acetate/acetic acid (pH 3, 3.5, 4, 4.5, 5, and 5.5), MES/NaOH (pH 6 and 6.5), HEPES/NaOH (pH 7 and 7.5), and Bicine/HCl (pH 8.0, 8.5, 9.0, 9.5, and 10.0) buffers. For cell permeabilization, the buffered medium was supplemented with 0.01% Triton X-100 (Sigma). After permeabilization, cells retained their fluorescence for ~30 min and did not exhibit significant morphological changes for pH values between 5 and 7.5. At longer times (>40 min), cells appeared rounded and lost their fluorescence because of the cytosolic washout of the construct.

Absorption Measurement. Recombinant proteins were diluted into buffers of the appropriate pH to give a final protein concentration of ~0.8 mg/mL. Spectra extending from 250 to 700 nm were measured on a NanoDrop spectrometer (Peqlab, Göttingen, Germany) and corrected for the appropriate blank. Furthermore, for pH <5, the absorption was corrected for scattering by subtraction of a const./λ^2 term. Finally, the spectra were normalized to unity at 443 nm by their absorption at 280 nm.

Cell Culture. Chinese hamster ovary (CHO), rat pheochromocytoma PC12, and mammary adenocarcinoma (MCF-7) cell lines were cultivated at 37 °C, 5% CO_2, and 80% humidity. The growth medium for CHO was composed of Dulbecco's modified Eagle's medium high-glucose containing glutamine (DMEM) and 10% (v/v) fetal calf serum (FCS) supplemented with 10000 IU of penicillin and streptomycin (P/S), all provided by PAA. Growth medium for PC12 consisted of DMEM, 10% horse serum (Sigma-Aldrich Chemie GmbH), 5% FCS, and 10000 IU of P/S. Growth medium for MCF-7 cells was DMEM supplemented with 5% FCS, 4.5 g/L pyruvate (Gibco, Invitrogen GmbH, Karlsruhe, Germany), and 10000 IU of P/S.

Cells were seeded in chambered borosilicate LabTek coverslips (Thermo Fisher Scientific-Nunc, Wiesbaden, Germany) and transfected after 24 h with pcDNA:pHlameleons using the Effectene reagent (Qiagen, Hilden, Germany) according to the protocol provided by the supplier. After 36−48 h, cells were rinsed and kept in imaging medium (125 mM KCl, 20 mM NaCl, 0.5 mM $CaCl_2$, and 0.5 mM $MgCl_2$). MCF-7 cells were transfected with Magnet Assisted Transfection (MATra; IBA GmbH, Göttingen, Germany) according to the instructions provided by the manufacturer.

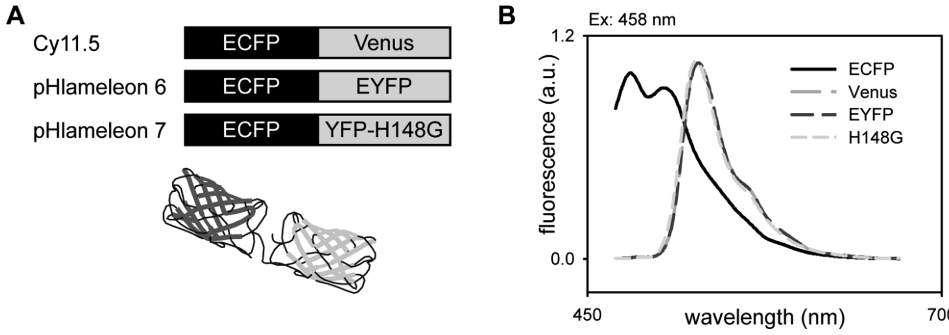

FIGURE 1: ECFP, YFPs, and pHlameleons. (A) Schematic representation of the Cy11.5 parent and the derived pHlameleons. (B) Emission spectra of ECFP, Venus, EYFP, and H148G expressed in PC12 cells.

Spectral Imaging. Spectral images were acquired using a TSC-SP2 AOBS (Leica Microsystems GmbH, Wetzlar, Germany) confocal microscope by using the 458 and 514 nm lines provided by the argon ion laser. Spectra were acquired using λ scans between 465 and 675 nm by the acquisition of 20 images that were 10 nm wide. Spectral imaging on cells was performed in the 473−593 nm range with 10 equidistant steps and 20 nm wide acquisitions to limit the exposure time. The corresponding fluorescence ratios were computed using the summed images between 486 ± 21 and 549 ± 21 nm for in vitro experiments and 491 ± 17 and 543 ± 17 nm for measurements in cell culture.

Frequency Domain Lifetime Imaging. Lifetime imaging was performed by an in-house-developed wide-field frequency domain lifetime imaging microscope (*14*). The 458 nm laser line of an Innova 300C argon ion laser (Coherent Inc., Santa Clara, CA) was used to excite ECFP. Lifetime images of the pHlameleons were acquired with a long pass 510 nm dichroic and a long pass 515 nm barrier filter (both from AHF Analysentechnik AG, Tübingen, Germany).

Imaging of Cytosolic Acidification by Lysosomal Disruption. Approximately 24 h after transfection, MCF-7 cells were treated with 50 μM *N*-dodecyl (C12) imidazole (Toronto Research Chemicals Inc., North York, ON), prepared by the method described by Firestone et al. (*15*). At 30 min intervals, cells were removed from the incubator and imaged on the frequency domain FLIM microscope setup at 24 °C for a maximum of 5 min, typically yielding 10 lifetime images per interval. Physiological temperature is critical for the lysosomal disruptive action of *N*-dodecyl (C12) imidazole as prolonged incubation at room temperature did not produce any acidification (data not shown). The lifetime image for each cell was stored, and the distribution of lifetime values of individual cells was statistically analyzed using automated routines written in-house for MatLab (Mathworks, Natick, MA). Further analysis, fitting, and data representation were performed using the IgorPro suite (Wavemetrics, Lake Oswego, OR). Lifetime distributions were normalized to the number of imaged pixels per cell, yielding probability density functions with an integrated value of unity.

RESULTS

Emission Spectra of ECFP and Different YFPs. Figure 1 shows the emission spectra of ECFP and the YFPs used for the cloning of the pHlameleon constructs. ECFP exhibits a typical spectrum with two emission peaks. The spectra shown were collected from proteins expressed in PC12 cells and at neutral pH. Venus and EYFP exhibited indistinguishable spectra, whereas the emission spectrum of H148G appears slightly blue-shifted. The absorption spectra of the pHlameleons are shown in Figure 2 for different pH values. The reduction of the molar extinction coefficient for the different YFP moieties at low pH values is apparent and in agreement with the respective ranges of pH sensitivity of their emission. See also Table 1 for a summary of the spectroscopic properties of ECFP and the YFPs used in this work.

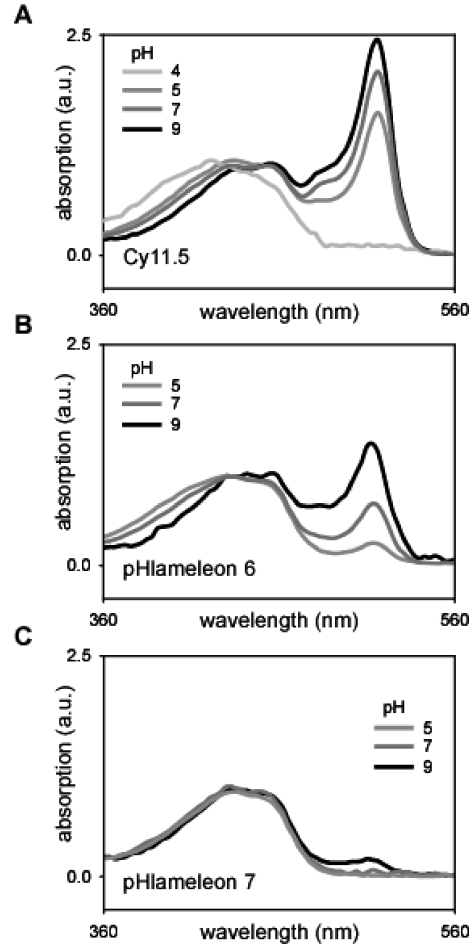

FIGURE 2: Absorption spectra of (A) Cy11.5, (B) pHlameleon 6, and (C) pHlameleon 7 at different pH values. Over the pH range of 5−9, the ECFP molar extinction coefficient is comparatively stable, while the YFPs exhibit the expected high pH sensitivity. The protonation of Venus (see Cy11.5 in panel A) occurs significantly only at a lower pH of ~4.

Characterization of Cy11.5. For pH ≥5.5, Cy11.5 exhibits the characteristic emission spectrum of Venus with a residual blue tail emission from ECFP. Spectral analysis revealed that

Table 1: Spectral Characteristics of ECFP and YFPs

	$\lambda_{ex}/\lambda_{em}$ (nm)	Φ	ε ($\times 10^3$ M^{-1} cm^{-1})	pK_a	fluorescence lifetime[a] (ns)	ref[b]
ECFP	434/474	0.36	28	4.8	2.3/3.0	*10*
Venus	515/528	0.57	92.2	6.0	2.9/3.0[d]	*8*, *10*
EYFP	515/528	0.61	80.4	6.9	3.0/3.0[d]	*8*
H148G	512/528	not available	~6[c]	7.9	2.1/2.6[d]	*9*

[a] Fluorescence lifetime is indicated as phase lifetime estimator/modulation lifetime estimator. [b] Primary reference. [c] This work. [d] Excitation at 501 nm and emission at >515 nm.

Cy11.5 exhibited ~85% energy transfer. The FRET efficiency of 98% originally reported (*11*) was inferred from the quenching efficiency as judged by the ratio of the shortest decays to the longest decay of ECFP. The lower ~85% value is the practical apparent value that is measured on an ensemble of fluorophores where different states of the biosensors may exist, e.g., the presence of misfolded acceptors (*11*) or a FRET-incompetent electronic state of the donor (*11, 16*). Originally, Cy11.5 was generated to provide a large Stokes shift fluorophore based on FRET; therefore, Cy11.5 was optimized to exhibit a reduced sensitivity to pH by the use of Venus, a YFP whose pK_a is equal to ~6.0 (*8*).

At a pH lower than 5.5, Cy11.5 emission spectrum gradually switches to the typical ECFP emission because of the negligible spectral overlap of the absorption of the protonated Venus chromophore with the ECFP emission spectrum and the consequent dequenching of the donor fluorescence. Figure 3A shows the pH dependence of the emission spectrum of Cy11.5 and a remarkable pH sensitivity of the ratio of fluorescence at 481 and 533 nm with an apparent pK_a of 4.1 ± 0.1 and a high Hill coefficient of 1.8 ± 0.3. The iso-emissive point is not ideally defined because of the modulation of the relative weights of the two emission peaks of ECFP at different pH values. The relative variation of the ECFP (481 nm) and Venus (533 nm) emission was estimated by the fractional contribution to the spectra and showed the quenching of the protonated Venus chromophore accompanied by the ECFP dequenching (Figure 3B). Because of these two concomitant events, the apparent pK_a of the two proteins converges to ~4.9 (see also Table 2 and the Appendix).

pK_a Tuning and Characterization of pHlameleons. Cy11.5 could be used as a very sensitive (i.e., it exhibits a large Hill coefficient) ratiometric pH biosensor for low pH, for instance, to report on intralysosomal changes. In line with the naming of our other sensors, we also refer to this protein as pHlameleon 5 (for its pK_a). However, most physiological pH variations occur at higher values. Figure 3C−F shows the pH-dependent spectral shift of Cy11.5 when Venus is replaced with EYFP (Figure 3C,D) and H148G (Figure 3E,F). EYFP and H148G were selected because of their pK_a values being higher than that of Venus, i.e., 6.9 and 7.9 (*8*), respectively. The ECFP−EYFP fusion construct, called pHlameleon 6, exhibits an apparent pK_a of 5.80 ± 0.06 and a Hill coefficient of 0.83 ± 0.09. pHlameleon 6 is thus sensitive over an acidic pH range (5.0−7.5) that is highly physiologically relevant. The apparent pK_a of ECFP and EYFP was equal to ~6.3. The overall conformation of Cy11.5 and pHlameleon 6 should not differ, but a slight loss of FRET of the nonprotonated biosensor (from ~85 to 70%) was detected as a consequence of a lower extinction coefficient of EYFP compared to Venus (see Figure 2A,B and the Appendix).

The loss of energy transfer was almost complete (FRET efficiency of ~3%) for the ECFP−H148G fusion construct (pHlameleon 7), rendering pHlameleon 7 inefficient for spectral imaging under the experimental conditions shown here. However, the pH-dependent spectral modulation of ECFP is still apparent, and the H148G fluorescence emission shifts the peak of the emission spectrum to higher wavelengths due to the direct excitation of the fluorophore.

Characterization of pHlameleon in Cell Culture. Cy11.5 and pHlameleon 6 were expressed in CHO cells, whose cytosolic pH was buffered by a mild permeabilization protocol and the use of pH-adjusted extracellular media. Cells appeared viable within pH 5−7.5 for ~20−30 min, whereas their phenotype changed immediately at pH 4−4.5 and 8−8.5. Therefore, no images were collected at a pH lower than 4 and higher than 8.5. The spectral shift of the pHlameleons measured in cells was consistent with that measured in vitro, demonstrating their potential use for biologically relevant applications. In cells, the spectral shift of Cy11.5 exhibited a pK_a of 4.41 ± 0.09 and a Hill coefficient of 1.9 ± 0.6, with apparent pK_a values for ECFP and Venus emission of 5.0 ± 0.2 and 4.7 ± 0.2, respectively. Under the same experimental conditions, pHlameleon 6 exhibited a pK_a of 5.58 ± 0.09 and a Hill coefficient of 1.0 ± 0.2, with apparent pK_a values for ECFP and EYFP emission of 5.9 ± 0.2 and 6.0 ± 0.2, respectively.

Fluorescence Lifetime Detection of pH by pHlameleon Acceptor In-Growth. The reduction of the donor quantum yield at low pH hampers donor lifetime imaging of the pHlameleons. Therefore, pHlameleons were characterized by acceptor in-growth, where the mixed fluorescence of both the donor and acceptor is detected by frequency domain lifetime imaging (*17*). Figure 5 shows the application of lifetime detection for the bead-conjugated pHlameleons. Notably, in spite of its reduced dynamic range due to the significant loss of FRET, pHlameleon 7 can still be used for pH sensing thanks to the pH-dependent quantitative mixing of the ECFP and H148G lifetimes.

Cy11.5 (Figure 5A) exhibited a pK_a of 4.76 ± 0.03 and a large Hill coefficient of 2.8 ± 0.3. Phase and modulation lifetime estimations diverge at low pH and converge to similar values under more alkaline conditions. The pK_a of pHlameleon 6 shifted to 6.2 ± 0.1 with a Hill coefficient equal to 0.8 ± 0.1. Although showing a trend similar to that with Cy11.5, the phase and modulation lifetimes approach the average lifetime estimation to a lesser degree. The two lifetime estimations do not converge for pHlameleon 7, which can still be adequately used for pH sensing with a pK_a of 7.1 ± 0.1 and a Hill coefficient of 0.8 ± 0.1. We note that in the absence of photons generated by excited-state reactions (like FRET), the modulation lifetime is always greater than, or equal to, the phase lifetime (*18*) and the difference between the two estimations is related to lifetime heterogeneity (*14*). This can be appreciated from the plots in Figure 5 at low pH values, where no FRET occurs. Under more alkaline conditions, FRET reduces lifetime heterogeneity and the phase and modulation estimators converge. In the case of pHlameleon 7, it is apparent that no FRET is occurring and that the pH-dependent shift of the fluorescence lifetime reflects only the combination of fluorescence emission of

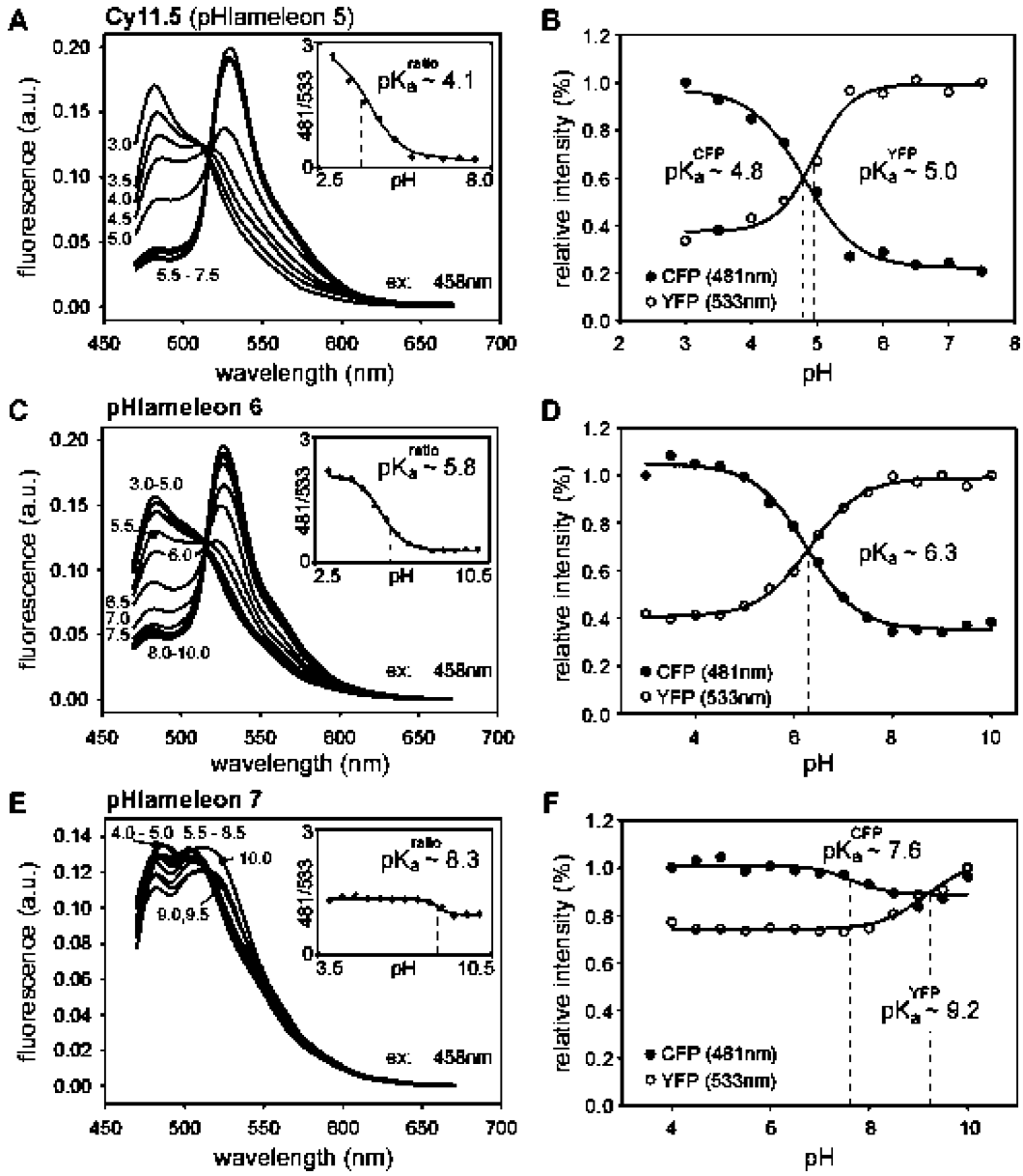

FIGURE 3: Spectral characterization of bead-conjugated pHlameleons. (A, C, and E) Emission spectra as a function of pH using excitation at 458 nm. The inset shows the ratio of fluorescence emission measured at 481 and 533 nm. (B, D, and F) Fluorescence intensities of ECFP and Venus, EYFP, and H148G within the different pHlameleons vs pH. Spectra were normalized to their integral value.

cyan and yellow fluorescent proteins. Notably, the apparent pK_a values measured with various estimators (intensity ratios and phase, modulation, and average lifetimes) differ from each other, as the estimators differently weigh the heterogeneous emission of the donor−acceptor biosensor (see the Appendix).

pH Imaging. Figure 6A,B shows images of CHO cells expressing pHlameleon 6 and the ratio of donor to acceptor fluorescence. Sensitized emission detection usually requires calibration for spectral bleed-through, direct excitation of the acceptor, and normalization of the FRET index to the apparent donor and/or acceptor concentration. Since pHlameleon is a fusion construct of both the donor and acceptor and thus provides a fixed stoichiometry, the emission ratio can be used directly as the pH index. Occasionally, the nontargeted pHlameleons expressed in cell culture without permeabilization can become localized in lysosomes (data not shown), leading to inhomogeneity in the FRET ratios due to the low pH of these organelles.

Figure 6C,D shows images of PC12 cells expressing pHlameleon 6 and imaged by FD-FLIM. The conformity of the FRET ratio and lifetime shown in panels B and D of Figure 6 indicates that both techniques are equally suitable for the quantitative readout of pH.

Cytosolic Acidification by Lysosomal Disruption. The applicability of the pHlameleon sensor approach was shown by the investigation of the acidification of the cytosol upon disruption of lysosomes. Loss of lysosomal integrity has been associated with apoptotic and necrotic cell death (*19*−*21*). We measured the cytosolic pH of MCF7 cells expressing pHlameleon 6 by the lifetime of the EYFP moiety upon excitation of ECFP. As this measurement is intrinsically calibrated, it is possible to convert the lifetime values to pH values by inversion of the Hill equation, using the parameters obtained from the calibration experiment shown in Figure 5B. Lysosomal leakage was induced by incubation with 50 μM *N*-dodecyl (C12) imidazole, a potent lysosomotropic detergent. The cell death outcome for this toxic treatment

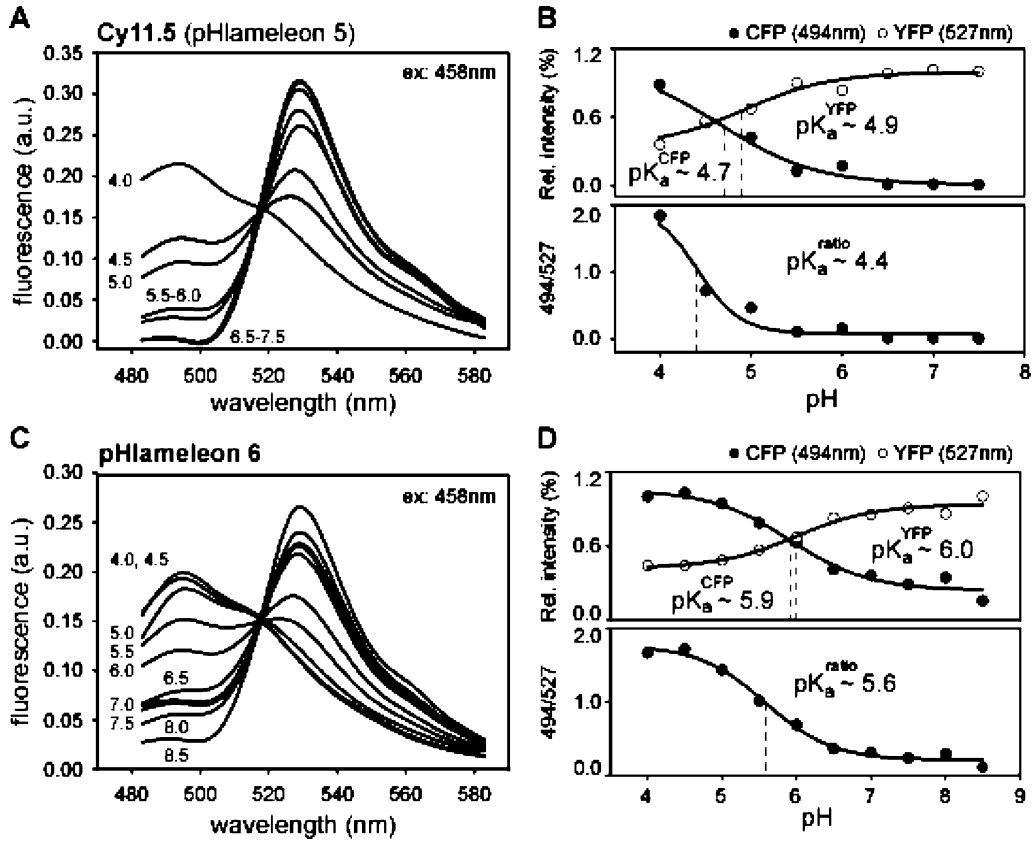

FIGURE 4: Spectral response of Cy11.5 (A and B) and pHlameleon 6 (C and D) in CHO cells.

Table 2: pH Sensitivity of pHlameleons

	spectral imaging		lifetime imaging	
	CFP pK_a, YFP pK_a	ratio pK_a, ratio n_h	τ_ϕ pK_a, τ_m pK_a	τ_a pK_a, τ_a n_h
Cy11.5 (pHlameleon 5)	4.80 ± 0.09	4.1 ± 0.1	4.69 ± 0.04	4.76 ± 0.03
	4.95 ± 0.08	1.8 ± 0.3	4.80 ± 0.03	2.8 ± 0.3
pHlameleon 6	6.25 ± 0.06	5.80 ± 0.06	5.9 ± 0.1	6.2 ± 0.1
	6.32 ± 0.05	0.83 ± 0.09	6.5 ± 0.1	0.8 ± 0.1
pHlameleon 7	7.6 ± 0.4[a]	8.34 ± 0.09[a]	6.7 ± 0.2	7.1 ± 0.1
	9.2 ± 0.3[a]	1.6 ± 0.4[a]	7.4 ± 0.1	0.8 ± 0.1

[a] Spectral variations are not significant.

depends on the rate of lysosomal rupture, i.e., on the dose used. Here, a high concentration was used to drive cells into necrosis in a relatively short time (<5 h). Before and after the incubation, an untreated control sample was used to demonstrate the native, unperturbed, cytosolic pH of MCF7 cells and the stability of the microscope over the long incubation time. Figure 7A shows the pH, measured in individual control cells (○) and treated cells (●), at the indicated time points. Figure 7B shows the lifetime distribution of individual cells that are correspondingly marked in Figure 7A. At each time point, averages and standard errors are shown for both control cells (□) and treated cells (■).

The control cells show some heterogeneity in cytosolic pH between cells, with an average pH of 7.14 ± 0.07 (mean ± the standard error of the mean; $N = 24$). This value is in good agreement with the value of 7.2 found by others (*22, 23*). The heterogeneity might be explained by variations in metabolic status or cell cycle. Figure 7B shows that the cytosolic pH for each individual cell can be determined with great accuracy due to the purely Gaussian shape of the distributions; the fitted lifetime value is equal to 2.7 ± 0.2 ns (mean ± the standard deviation, cell 1). The other cells have similar distribution widths. Incubation with *N*-dodecyl (C12) imidazole induced a significant reduction in YFP lifetime, indicative of acidification of the cytosol. The first measurement point around 30 min shows a pH distribution that is equal to the control. However, after 60 min, significantly (Figure 7; with a *t* test, $*p < 0.05$ and $**p < 0.01$) lower pH values are detected for the individual cells. A trend toward a new lower average pH at 6.66 ± 0.07 (mean ± the standard error of the mean; $N = 25$) can be estimated from the pooled average of the values comprised between 210 and 250 min.

DISCUSSION

Protonation of fluorescent proteins is a slow process compared with their excited-state lifetime. The protonation event and the consequent absorption shift in YFP require the diffusion of the proton to the chromophore (facilitated only in H148G) with a subsequent conformational rearrangement of the chromophore and the surrounding amino acids. These events occur on the microsecond time scale, 3 orders of magnitude slower than the fluorescence lifetime of

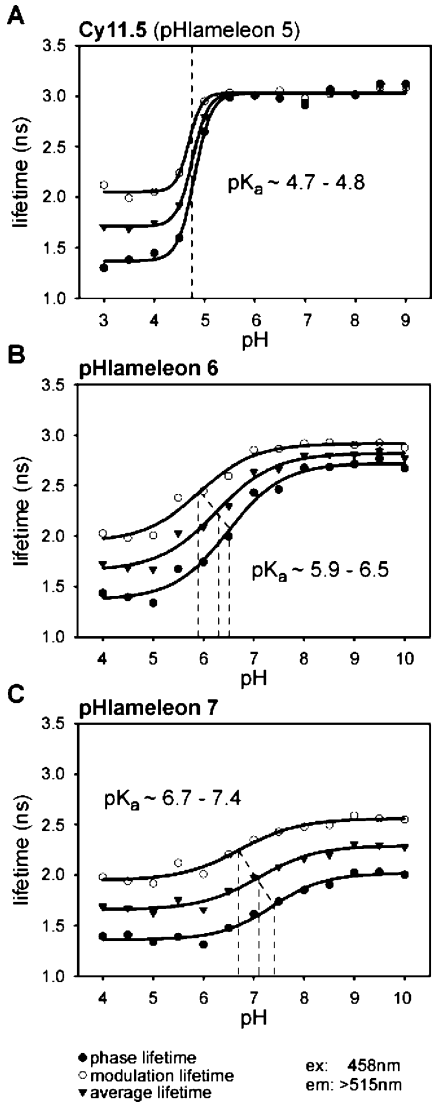

FIGURE 5: Fluorescence lifetime response of bead-conjugated pHlameleon to pH changes. (A−C) Apparent fluorescence lifetime of pHlameleon 5, 6, and 7, respectively. Combined donor and acceptor fluorescence emission was acquired with a long pass filter (>515 nm). Phase (●), modulation (○), and average (▼) lifetime estimations are shown.

fluorescent proteins (*24*). It can thus be assumed that energy transfer can be modeled as the modulation of the populations of protonated and nonprotonated fluorophores. At the single-molecule level, the protonation event renders the spectral overlap between donor and acceptor negligible, effectively preventing energy transfer (see the Appendix).

Many fluorescent proteins that sense diverse biochemical parameters, such as redox buffering, chaperone activities, phosphorylation, and pH, are available. Biosensors based on changes in molar extinction coefficient or fluorescence quantum yields cannot, in general, be read out quantitatively by their change in fluorescence emission intensity. However, fusion constructs exhibiting energy transfer can be used to generate ratiometric probes that exploit the variation of the spectroscopic properties of the donor and acceptor: FRET transfers energy from the donor to the acceptor but transfers information on the state of the acceptor, the protonation state for the pHlameleon, back to the donor.

The Cy11.5 protein was used as a template to generate pHlameleon 6 that made pH-dependent variations of CFP and YFP fluorescence in the physiological range quantitatively accessible. The design of Cy11.5 was also adopted to ensure high pH sensitivity caused by the pH-dependent FRET frustration process and the high resistance to protease activity offered by the short linker between the donor and acceptor. Even though the loss of energy transfer rendered pHlameleon 7 inefficient for spectral imaging, it is still applicable for lifetime detection and for imaging with dual excitation (data not shown). Co-expression of ECFP and EYFP was used previously for pH sensing. However, the control over the expression level of the two proteins is limited, and this required the calibration of this assay for every measured cell. Even in the absence of FRET, a fusion construct like pHlameleon 7 retains the advantage of not requiring such a single-cell assay calibration routine.

Therefore, this design allowed the construction of the pHlameleons, the Cy11.5 itself, and two other fusion constructs, exhibiting an apparent pK_a between 5 and 8. The high intramolecular FRET efficiency occurring in Cy11.5 appears to further increase its pH shift, providing a very large Hill coefficient. pHlameleon 6 was cloned to shift the apparent pK_a toward a higher pH range. The substitution of EYFP for Venus resulted in the expected pK_a tuning but was accompanied by a moderate decrease in the rate of energy transfer. This reduced the Hill coefficient of pHlameleon 6 compared to that of Cy11.5 to the benefit of permitting its use over the physiological pH range.

To extend the pH sensing range, the H148G mutation was introduced into pHlameleon 6. This resulted in the expected shift of the pK_a to ~7 but also caused a further loss of energy transfer. Because of the sixth-root dependence of R_0 on the molar extinction coefficient, and the very high FRET efficiency exhibited by the original Cy11.5 construct, differences in the molar extinction coefficients of the different YFPs may not have a dramatic effect on the FRET efficiency of pHlameleons (see the Appendix); however, it can be inferred from Figure 2 that the molar extinction coefficient of EYFP-H148G is diminished to an extent (more than 1 order of magnitude) that renders the spectral overlap with ECFP negligible.

In our designs, we focused on increasing the low pK_a of Cy11.5 and did so by inclusion of a known pH-destabilized YFP form. More YFP variants should be tested to yield a sensor that still exhibits the favorable high FRET coupling that confers high sensitivity. The modular nature of the pHlameleon sensing platform facilitates this search.

In our experimental setup, we used the laser line of an argon ion laser that peaked at 458 nm. At this wavelength, direct excitation of EYFP cannot be neglected, also because of the comparatively lower quantum yield of ECFP, i.e., ~0.4 for ECFP versus ~0.6 for EYFP (*8*). The dynamic range of the pHlameleons could thus be higher than those presented in this work when the 430 nm laser line that is currently available is used.

It should be noted that fluorescent proteins are sensitive to the concentration of halide ions. This property is exploited in the FRET-based biosensor Clomeleon to sense the chloride concentration (*25*). Moderate variations in cytosolic pH (±0.2 pH unit around 7.4) can cause a 40% error in the estimation of chloride concentrations (*13*); nevertheless, the Clomeleon is reported to be a poor lifetime pH sensor because its fluorescence lifetime does not unequivocally depend on pH

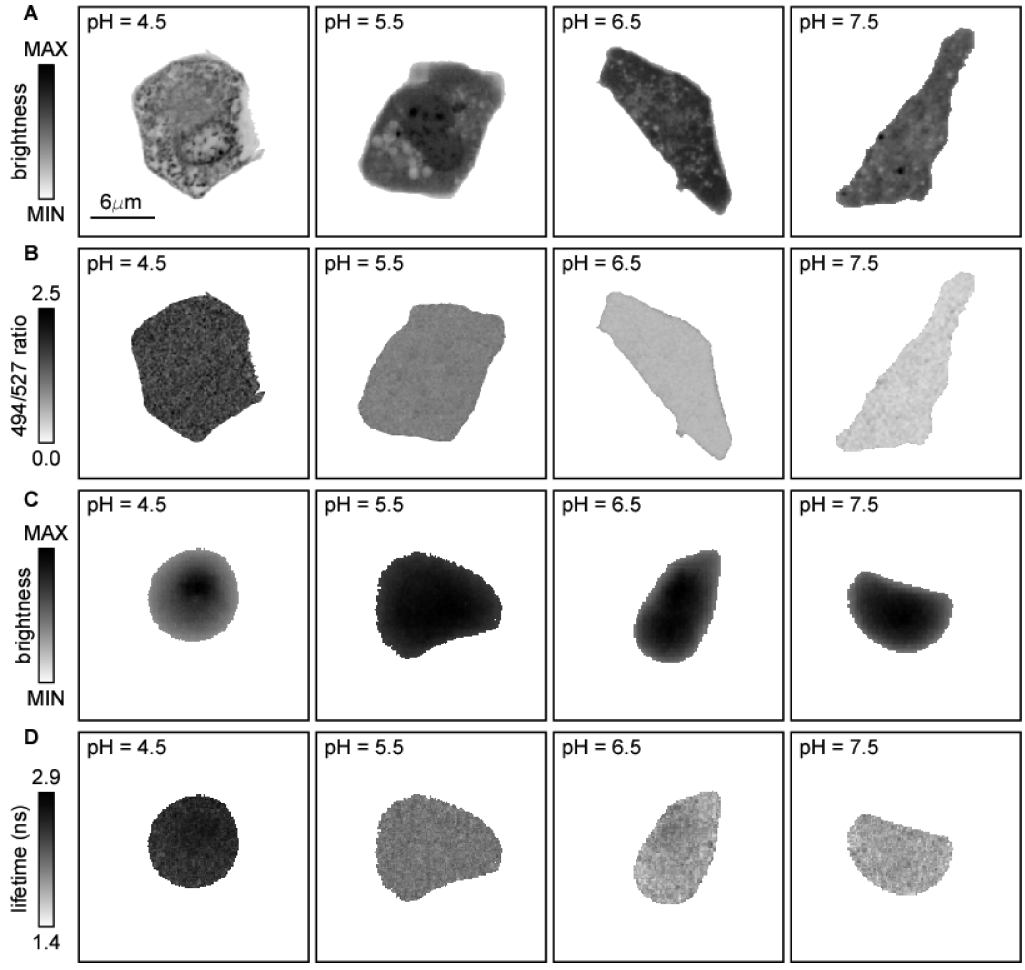

FIGURE 6: Imaging intracellular pH with pHlameleon 6. (A and B) Confocal images of CHO cells expressing pHlameleon 6 where the cytosolic pH was buffered at the different indicated pH values: (A) average intensity images computed over the entire emission spectrum and (B) fluorescence emission ratios of 494 to 527 nm. (C and D) Wide-field FD-FLIM images of PC12 cells expressing pHlameleon 6 at different pH values: (C) average intensities and (D) apparent fluorescent lifetimes of pHlameleon 6.

(*25*). Although pHlameleons and other biosensors that are based on CFP and YFP may benefit from future optimization to exhibit a reduced sensitivity to halide ions, the cross-talk between chloride and pH should be negligible for a pH biosensor as (i) physiologically, chloride concentrations vary significantly only during neuronal development and, in general, only in excitable cells and (ii) typical intracellular chloride concentrations for mammalian cells are in the millimolar range, i.e., 1 order of magnitude lower than the typical chloride pK_d values (100−200 mM) for YFPs (*13, 26*).

Figure 6 shows that pHlameleons can provide reliable pH detection in different cell types, and with different techniques. The advantage of lifetime imaging is that it mostly depends on the molecular properties of the probes, making it a self-referenced detection technique that requires less (or even no) external calibration (*27*−*29*). On the other hand, it has to be noted that sensitized emission provides a fast readout that is compatible with most imaging setups.

The possibility of following comparatively small pH variations in living cells was shown by the use of *N*-dodecyl (C12) imidazole. Three things are evident from this experiment. (i) There is a statistically significant drop in cytosolic pH with *N*-dodecyl (C12) imidazole treatment. (ii) The excursion of the cytosolic pH in cells with compromised lysosomal integrity is skewed in the direction of lower pH. Representative distributions for individually marked cells are shown in Figure 7B. Cell 5 exhibits the lowest pH. (iii) After incubation for 5 h, the pH rapidly returns to physiological values for most cells. This is indicative of a loss in plasma membrane permeability, and quick equilibration of the cytosolic pH with the buffered medium, which is typical for necrotic cell death. Due to this competitive process, we cannot exclude the possibility that the pH excursions are, in fact, larger at the later time points of treatment.

The acidification of *N*-dodecyl (C12) imidazole-treated cells coincides with morphological changes typical for necrosis (see the Supporting Information), a clearer definition of the cell nucleus, cellular rounding, and swelling and eventually a spherical morphology with loss or dilution of cytosolic material.

Incubation with the Vital Dye Lysotracker Red Shows That the Rounding Phase Coincides with the Onset of Lysosomal Leakage. The reason for the increased heterogeneity in pH response per cell remains unclear. Our results seem to suggest that cells have different susceptibilities for lysosomal leakage, perhaps due to differences in uptake rates, lysosomal membrane composition, cytosolic pH buffering capacity, expression levels of individual cathepsins that might contribute to lysosomal membrane leakage, and other metabolic factors. Understanding the basis of this heterogeneity might have important consequences for increasing tumor cell susceptibility for cancer treatments or improving the cell

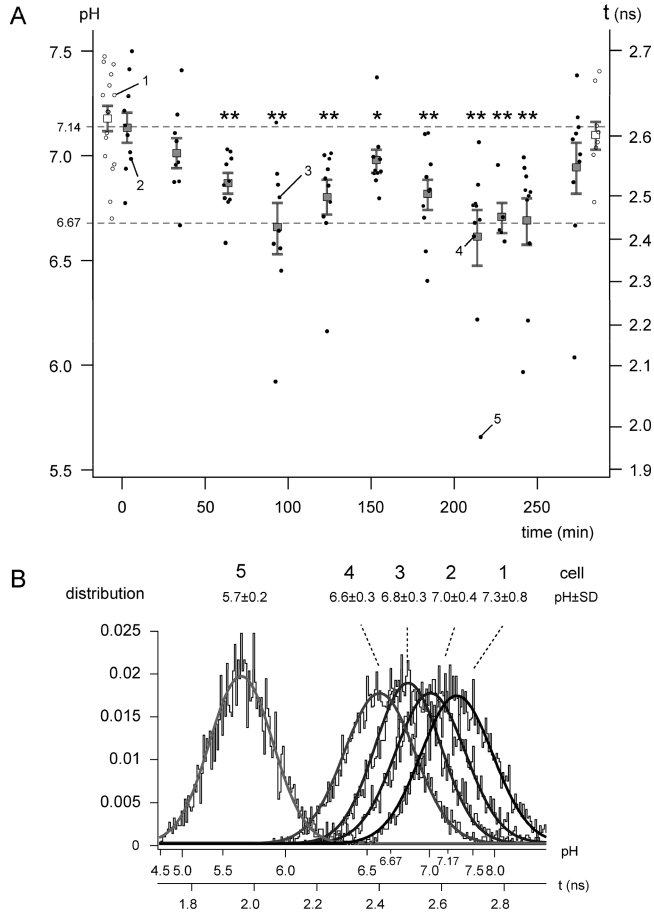

FIGURE 7: Imaging cytosolic acidification of MCF7 upon lysosomal disruption. (A) Lifetimes and calculated pH values of MCF7 cells treated with *N*-dodecyl (C12) imidazole for the indicated time points (●). Control cells that were not treated (○) were measured before the start and at the end of the experiment. Squares and error bars indicate averages and standard errors for each time point, respectively; during lysosomal disruption, acidification was statistically significant: $*p < 0.05$, $**p < 0.01$. Gray lines represent the average of the pH controls (top) and the average final pH reached between 210 and 250 min. (B) Lifetime distribution and calculated lifetimes of the five cells that are described in panel A.

viability outcome in stroke and neurodegenerative disease. This pronounced heterogeneity is also observed when individual cells are followed; the pH switches relatively steeply, but with variable onset [as judged by ratio measurements (data not shown)]. The global response of the cell population to the treatment shown in Figure 7A thus mainly represents the pH transition, i.e., the lysosomal "opening" probability.

Here, we wanted to show the capability and reliability of our new sensor design in accurately determining, on a cell-by-cell basis, the intracellular pH during a defined necrotic cell death stimulus. Other studies have shown that cell death involves lysosomal leakage and corresponding cytosolic acidification; Syntichaki et al. (*30*) show by expression of a pH-sensitive GFP variant that necrotically swollen touch receptor sensory neurons of the nematode *Caenorhabditis elegans* have an acidic cytosol but did not quantify the pH changes. Using the pH-sensitive dye BCECF [2′,7′-bis(2-carboxyethyl)-5(6)-carboxyfluorescein], the cytosolic pH upon induction of apoptosis of U397 cells by TNFα was followed by dual emission ratiometric flow cytometry (*22*). The cytosol was found to be acidified from pH 7.2 to 5.8, similar to the necrotic changes shown here. Our imaging approach is gentle to adherent (or tissue) cells, which is important when following cell death progression, uses measurements at one emission wavelength that are intrinsically calibrated, and can be automated for the measurement of large numbers of cells (*31*), comparable to flow cytometry.

CONCLUSIONS

The presented pHlameleons are prototypes of a new class of pH sensors that can be further optimized, tuned, and targeted to different subcellular structures or attached to target proteins to interrogate pH changes in cellular microdomains. pHlameleons possess ideal properties for intracellular pH measurements; they provide highly enhanced spectral dynamics compared to previous genetically encodable biosensors and offer fast and quantitative detection, with all the flexibility of genetically encodable biosensors.

Our use of the design of Cy11.5, with its high FRET efficiency and protease resistance, shows that it can offer the basis for the construction of other biosensors that are based on spectral overlap engineering using concepts that are similar to those of the pHlameleons.

APPENDIX: THEORY

The Förster distance (R_0) is the characteristic interchromophore distance of a FRET pair at which the donor transfers 50% of its energy to the acceptor. R_0 can be expressed as a function of the spectral overlap integral (J), the quantum yield

of the donor fluorophore (Q_D), an orientational factor (k^2), and the refractive index of the medium:

$$R_0 = 0.211\sqrt[6]{\frac{\kappa^2}{n^4}Q_D J} \quad (\text{in Å})$$

The spectral overlap integral is defined by

$$J = \frac{\int F(\lambda)\varepsilon_A(\lambda)\lambda^4\,d\lambda}{\int F(\lambda)\,d\lambda} \quad (\text{in } M^{-1}\,cm^{-1}\,nm^4)$$

where $F(\lambda)$ is the fluorescence emission of the donor and $\varepsilon_A(\lambda)$ the molar extinction of the acceptor. For the computation of J, pH variations of the molar extinction coefficient of the acceptor, where $F(\lambda)$ is negligible, are not relevant.

The FRET efficiency, i.e., the relative energy transferred from the donor to acceptor, is equal to

$$E = \frac{k_T}{k_D + k_T};\quad k_T = k_D\left(\frac{R_0}{R}\right)^6 \Rightarrow E = \frac{1}{1+\left(\frac{R}{R_0}\right)^6}$$

Variations in the spectral overlap (J') compared to a reference state (J) cause variations in energy transfer:

$$E = \frac{1}{1+\frac{J}{J'}\left(\frac{1}{E_0}-1\right)}$$

Substituting YFP in the Cy11.5 fusion construct caused a reduction in the FRET efficiency. Because of the structural equivalence of the YFPs used in this work, differences in intermolecular distance or in the orientation are unlikely; compared to Venus, the EYFP and H148G mutants exhibit ~1.8- and ~15-fold (see Figure 2) decreases in absorption (and therefore spectral overlap), respectively. Therefore, the equation given above justifies the 76% and negligible FRET efficiency measured under alkaline conditions for pHlameleons 6 and 7, respectively.

The protonation of the chomophore of a fluorescence protein is slower than its fluorescence decay. Therefore, the apparent FRET efficiency of a pHlameleon can be approximated by the apparent FRET efficiency averaged over the protonated and nonprotonated molecular fractions:

$$E = (1-\alpha_{AH})E_0 + \frac{\alpha_{AH}}{1+\frac{J_0}{J_{AH}}\left(\frac{1}{E_0}-1\right)} = E_0\left[1-\alpha_{AH}\frac{(1-E_0)\left(1-\frac{J_{AH}}{J_0}\right)}{1-E_0\left(1-\frac{J_{AH}}{J_0}\right)}\right]$$

where

$$\alpha_{AH} = [1+10^{-n_{h,A}(pK_a^A-pH)}]^{-1}$$

is the molecular fraction of protonated acceptors. We have shown experimentally that the pH sensitivity of pHlameleons is tuned to different pH ranges because of substitutions of acceptors that exhibit different pK_a values.

This formalism illustrates the mechanisms by which spectral overlap engineering can be used to alter energy transfer efficiency and to generate different biosensors. However, the description of the fluorescence emitted by an ensemble of donor−acceptor pairs at different pH values is more complex. The number of fluorescent emitters is a stochastic ensemble of pHlameleons with only protonated donor (DHA), protonated acceptor (DAH), protonated donor and acceptor (DHAH), and nonprotonated fluorophores (DA). Donors (D and DH) emit over both donor and acceptor spectral bands, while acceptors (A and AH) emit only in the acceptor channel. Typically, the protonated form of YFPs is nonfluorescent in the spectral range relevant for this work. For each protonated species, the energy transfer will be frustrated (*32, 33*) by a fraction equal to the $1 - f_H$ quantity because of the reduction in spectral overlap ($\Delta = J_H/J_{DA}$, with H being DHA, DAH, or DHAH) or because of the reduction in the donor quantum yield ($\Delta = Q_{DH}/Q_D$):

$$E_H = E_0\frac{\Delta}{1-(1-\Delta)E_0} = E_0 f_H$$

Each molecular fraction can be described by products of Hill functions:

$$\alpha_{DA} = [1+10^{n_{h,D}(pK_a^D-pH)}]^{-1}[1+10^{n_{h,A}(pK_a^A-pH)}]^{-1}$$

$$\alpha_{DHA} = 10^{n_{h,D}(pK_a^D-pH)}[1+10^{n_{h,D}(pK_a^D-pH)}]^{-1}[1+10^{n_{h,A}(pK_a^A-pH)}]^{-1} \approx 0$$

$$\alpha_{DAH} = 10^{n_{h,A}(pK_a^A-pH)}[1+10^{n_{h,D}(pK_a^D-pH)}]^{-1}[1+10^{n_{h,A}(pK_a^A-pH)}]^{-1}$$

$$\alpha_{DHAH} = 10^{n_{h,A}(pK_a^A-pH)+n_{h,D}(pK_a^D-pH)}[1+10^{n_{h,D}(pK_a^D-pH)}]^{-1}[1+10^{n_{h,A}(pK_a^A-pH)}]^{-1}$$

For a biosensor where the donor exhibits a pK_a lower than that of the acceptor, α_{DHA} will be always negligible. Figure 8A shows the pH dependence of the molecular fractions: the pHlameleons smoothly switch between three different states (DHAH → DAH → DA) going from low to high pH values.

The total fluorescence emission of donor fluorophores can be thus described as the sum of fluorescence emission of the molecules at different protonation states:

$$I_D = I^{DO}{}_{DA}(1-E_0) + I^{DO}{}_{DAH}(1-f_{DAH}E_0) + I^{DO}{}_{DHAH}(1-f_{DHAH}E_0)$$

For the pHlameleons, the energy transfer at any state where the acceptor is protonated (DAH and DHAH) is completely inhibited (f_{DAH} and $f_{DHAH} \sim 0$); therefore, donor fluorescence can be described by the simple equation

$$I_D \approx F^{D0}\left[\alpha_{DA}(1-E_0) + \alpha_{DAH} + \frac{Q_{DH}}{Q_D}\alpha_{DHAH}\right]$$

For an ideal FRET-based biosensor ($E_0 = 1$, and $Q_{DH} = Q_D$), the donor intensity is directly proportional to the protonation state of the acceptor:

$$I_D \approx F^{D0}(\alpha_{DAH} + \alpha_{DHAH}) = F^{D0}\alpha_{AH} = F^{D0}\times 10^{n_{h,A}(pK_a^A-pH)}[1+10^{n_{h,A}(pK_a^A-pH)}]^{-1}$$

The pH sensitivity of the acceptor is effectively transferred to the donor fluorophore by means of the FRET channel, without compromising the signal-to-noise ratio at low pH

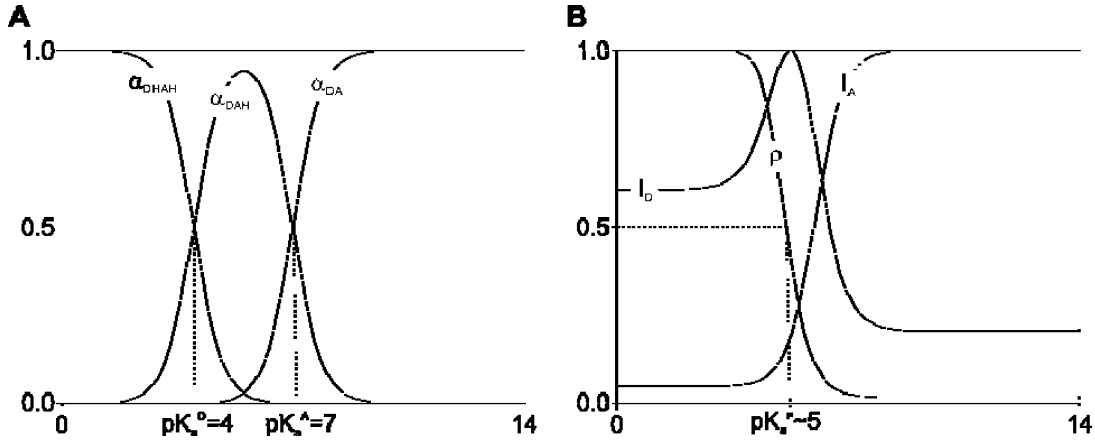

FIGURE 8: Numerical predictions for the protonation state (A) and fluorescence emission (B) of Cy11.5. See the text for a definition of symbols.

which is the case for ecliptic pH biosensors. For a typical ecliptic biosensor ($E_0 = 0$, and $Q_{DH} = 0$), the donor intensity is indeed inversely proportional to the protonation state of the donor:

$$I_D \approx F^{D0}(\alpha_{DA} + \alpha_{DAH}) = F^{D0}\alpha_D = F^{D0}[1 + 10^{n_{h,D}(pK_a^D - pH)}]^{-1}$$

Therefore, there is a substantial advantage for sensing the acidification of cells and organelles by the use of a FRET-based pH sensor with an ecliptic acceptor. In this case, the fluorescence of the acceptor fluorophore is

$$I_A \approx F^{A0}\alpha_{DA}(E_0 + de) = F^{A0}[1 + 10^{n_{h,D}(pK_a^D - pH)}]^{-1}[1 + 10^{n_{h,A}(pK_a^A - pH)}]^{-1}(E_0 + de)$$

where de is a coefficient describing the direct excitation of the acceptor by the excitation light source of the donor. Unfortunately, donor fluorescence emission always mixes with the acceptor fluorescence. Therefore, it is necessary to take this spectral bleed-through (bt) into consideration; the total fluorescence emitted in the acceptor spectral band is thus

$$I_A = F^{A0}[\alpha_{DA}(E_0 + de) + bt I_D]$$

The ratio of the donor to acceptor fluorescence (ρ) will follow the relation

$$\rho = \rho_0\left[\frac{\alpha_{DA}(E_0 + de)}{\alpha_{DA}(1 - E_0) + \alpha_{DAH} + \frac{Q_{DH}}{Q_D}\alpha_{DHAH}} + bt\right]^{-1}$$

This equation is plotted in Figure 8B with parameter values selected to represent Cy11.5. The pH-dependent reduction of the quantum yield of ECFP competes with the FRET-induced dequenching at low pH values; however, this nonmonotonic variation in I_D is also compensated by the rapid loss of acceptor fluorescence which results in a sigmoidal-like trend in the ratio ρ. Therefore, the apparent pK_a of this estimator exhibits intermediate values when compared to the pK_a values of the donor and the acceptor alone.

In first approximation, there are three molecular species that emit in the spectral range of both the donor and acceptor and that possess different fluorescence lifetimes (τ_{DA}^D, τ_{DAH}^D, and τ_{DHAH}^D), and one additional species in the acceptor-only spectral band (τ_{DA}^A):

$$\tau_{DA}^D = (k_D + k_T)^{-1}; \quad \alpha_{DA}(k_D + k_T)$$

$$\tau_{DAH}^D = k_D^{-1}; \quad \alpha_{DAH}k_D$$

$$\tau_{DHAH}^D = k_{DH}^{-1}; \quad \alpha_{DHAH}k_{DH}$$

$$\tau_{DA}^A = k_A^{-1}; \quad \alpha_{DA}k_A[de - k_T/(k_D + k_T - k_A)]$$

where the second column shows the amplitudes of the respective exponential decays. In the presence of fluorescence heterogeneity, phase fluorometry provides lifetime estimates inferred from fluorescence modulation that are higher than estimates inferred from the phase delay (*14*). However, at the negative amplitudes of the decay associated with sensitized acceptor emission, $(\alpha_{DA}k_Ak_T)/(k_D + k_T - k_A)$ corresponds to a higher phase-derived lifetime than the modulation-derived estimate (*17*). Therefore, the fluorescence lifetime measurements (see Figures 5 and 6) show increased fluorescence lifetime values (from τ_{DHAH}^D to τ_{DA}^A) at higher pH values and a concomitant convergence of the fluorescence phase and modulation lifetime estimators caused by the competition between heterogeneity effects and the effects by excited-state reactions. The latter is not present for pHameleon 7 because of the lack of detectable FRET (Figure 5C). It should be noted that the analysis of fluorescence lifetime is even more complicated by the presence of an additional third lifetime component in the ECFP emission that arises from a state of the proteins that may also be incapable of undergoing energy transfer (*25*) (due to their lower quantum yield). This explains the high heterogeneity detected by FD-FLIM at low pH values.

SUPPORTING INFORMATION AVAILABLE

Morphological changes typical for necrosis induced by *N*-dodecyl (C12) imidazole (Figure 1). This material is available free of charge via the Internet at http://pubs.acs.org.

REFERENCES

1. Whitaker, J. E., Haugland, R. P., and Prendergast, F. G. (1991) Spectral and photophysical studies of benzo[c]xanthene dyes: Dual emission pH sensors. *Anal. Biochem. 194*, 330–344.
2. Lin, H.-J., Herman, P., Kang, J. S., and Lakowicz, J. R. (2001) Fluorescence Lifetime Characterization of Novel Low-pH Probes. *Anal. Biochem. 294*, 118–125.

3. Miesenbock, G., De Angelis, D. A., and Rothman, J. E. (1998) Visualizing secretion and synaptic transmission with pH-sensitive green fluorescent proteins. *Nature 394*, 192–195.
4. Hanson, G. T., McAnaney, T. B., Park, E. S., Rendell, M. E., Yarbrough, D. K., Chu, S., Xi, L., Boxer, S. G., Montrose, M. H., and Remington, S. J. (2002) Green fluorescent protein variants as ratiometric dual emission pH sensors. 1. Structural characterization and preliminary application. *Biochemistry 41*, 15477–15488.
5. Kuhn, Y., Rohrbach, P., and Lanzer, M. (2007) Quantitative pH measurements in *Plasmodium falciparum*-infected erythrocytes using pHluorin. *Cell. Microbiol. 9*, 1004–1013.
6. Abad, M. F., Di Benedetto, G., Magalhaes, P. J., Filippin, L., and Pozzan, T. (2004) Mitochondrial pH monitored by a new engineered green fluorescent protein mutant. *J. Biol. Chem. 279*, 11521–11529.
7. Llopis, J., McCaffery, J. M., Miyawaki, A., Farquhar, M. G., and Tsien, R. Y. (1998) Measurement of cytosolic, mitochondrial, and Golgi pH in single living cells with green fluorescent proteins. *Proc. Natl. Acad. Sci. U.S.A. 95*, 6803–6808.
8. Nagai, T., Ibata, K., Park, E. S., Kubota, M., Mikoshiba, K., and Miyawaki, A. (2002) A variant of yellow fluorescent protein with fast and efficient maturation for cell-biological applications. *Nat. Biotechnol. 20*, 87–90.
9. Elsliger, M. A., Wachter, R. M., Hanson, G. T., Kallio, K., and Remington, S. J. (1999) Structural and spectral response of green fluorescent protein variants to changes in pH. *Biochemistry 38*, 5296–5301.
10. Gadella, T. W., Jr., Kremers, G. J., Goedhart, J., and van Munster, E. B. (2006) Cyan and yellow super fluorescent proteins with improved brightness, protein folding, and FRET Forster radius. *Biochemistry 45*, 6570–6580.
11. Shimozono, S., Hosoi, H., Mizuno, H., Fukano, T., Tahara, T., and Miyawaki, A. (2006) Concatenation of cyan and yellow fluorescent proteins for efficient resonance energy transfer. *Biochemistry 45*, 6267–6271.
12. Miyawaki, A., Llopis, J., Heim, R., McCaffery, J. M., Adams, J. A., Ikura, M., and Tsien, R. Y. (1997) Fluorescent indicators for Ca^{2+} based on green fluorescent proteins and calmodulin. *Nature 388*, 882–887.
13. Kuner, T., and Augustine, G. J. (2000) A Genetically Encoded Ratiometric Indicator for Chloride: Capturing Chloride Transients in Cultured Hippocampal Neurons. *Neuron 27*, 447–459.
14. Esposito, A., Gerritsen, H. C., and Wouters, F. S. (2005) Fluorescence lifetime heterogeneity resolution in the frequency-domain by Lifetime Moments Analysis (LiMA). *Biophys. J. 89*, 4286–4299.
15. Firestone, R. A., Pisano, J. M., and Bonney, R. J. (1979) Lysosomotropic Agents. 1. Synthesis and Cytotoxic Action of Lysosomotropic Detergents. *J. Med. Chem. 22*, 1130–1133.
16. Bae, J. H., Rubini, M., Jung, G., Wiegand, G., Seifert, M. H., Azim, M. K., Kim, J. S., Zumbusch, A., Holak, T. A., Moroder, L., Huber, R., and Budisa, N. (2003) Expansion of the genetic code enables design of a novel "gold" class of green fluorescent proteins. *J. Mol. Biol. 328*, 1071–1081.
17. Harpur, A. G., Wouters, F. S., and Bastiaens, P. I. (2001) Imaging FRET between spectrally similar GFP molecules in single cells. *Nat. Biotechnol. 19*, 167–169.
18. Lakowicz, J. R., and Balter, A. (1982) Analysis of Excited-State Processes by Phase-Modulation Fluorescence Spectroscopy. *Biophys. Chem. 16*, 117–132.
19. Li, W., Yuan, X. M., Nordgren, G., Dalen, H., Dubowchik, G. M., Firestone, R. A., and Brunk, U. T. (2000) Induction of cell death by the lysosomotropic detergent MSDH. *FEBS Lett. 470*, 35–39.
20. Gewies, A., and Grimm, S. (2003) Cathepsin-B and cathepsin-L expression levels do not correlate with sensitivity of tumour cells to TNF-α-mediated apoptosis. *Br. J. Cancer 89*, 1574–1580.
21. Cirman, T., Oresic, K., Mazovec, G. D., Turk, V., Reed, J. C., Myers, R. M., Salvesen, G. S., and Turk, B. (2004) Selective disruption of lysosomes in HeLa cells triggers apoptosis mediated by cleavage of bid by multiple papain-like lysosomal cathepsins. *J. Biol. Chem. 279*, 3578–3587.
22. Nilsson, C., Johansson, U., Johansson, A. C., Kagedal, K., and Ollinger, K. (2006) Cytosolic acidification and lysosomal alkalinization during TNF-α induced apoptosis in U937 cells. *Apoptosis 11*, 1149–1159.
23. Nilsson, C., Kagedal, K., Johansson, U., and Ollinger, K. (2003) Analysis of cytosolic and lysosomal pH in apoptotic cells by flow cytometry. *Methods Cell Sci. 25*, 185–194.
24. Mallik, R., Udgaonkar, J. B., and Krishnamoorthy, G. (2003) Kinetics of proton transfer in a green fluorescent protein: A laser-induced pH jump study. *J. Chem. Sci. 115*, 307–317.
25. Jose, M., Nair, D. K., Reissner, C., Hartig, R., and Zuschratter, W. (2007) Photophysics of Clomeleon by FLIM: Discriminating Excited State Reactions along Neuronal Development. *Biophys. J. 92*, 2237–2254.
26. Jayaraman, S., Haggie, P., Wachter, R. M., Remington, S. J., and Verkman, A. S. (2000) Mechanism and cellular applications of a green fluorescent protein-based halide sensor. *J. Biol. Chem. 275*, 6047–6050.
27. Sanders, R., Draaijer, A., Gerritsen, H. C., Houpt, P. M., and Levine, Y. K. (1995) Quantitative Ph Imaging in Cells Using Confocal Fluorescence Lifetime Imaging Microscopy. *Anal. Biochem. 227*, 302–308.
28. Hanson, K. M., Behne, M. J., Barry, N. P., Mauro, T. M., Gratton, E., and Clegg, R. M. (2002) Two-Photon Fluorescence Lifetime Imaging of the Skin Stratum Corneum pH Gradient. *Biophys. J. 83*, 1682–1690.
29. Lin, H. J., Herman, P., and Lakowicz, J. R. (2003) Fluorescence lifetime-resolved pH imaging of living cells. *Cytometry,* 52A.
30. Syntichaki, P., Samara, C., and Tavernarakis, N. (2005) The vacuolar H^+-ATPase mediates intracellular acidification required for neurodegeneration in C. elegans. *Curr. Biol. 15*, 1249–1254.
31. Esposito, A., Dohm, C. P., Bahr, M., and Wouters, F. S. (2007) Unsupervised Fluorescence Lifetime Imaging Microscopy for High-Content and High-Throughput Screening. *Mol. Cell. Proteomics 6*, 1446–1454.
32. Esposito, A. (2006) Molecular and Cellular Quantitative Microscopy: Theoretical investigations, technological developments and applications to the neurosciences. Ph.D. Thesis, Utrecht University, Utrecht, The Netherlands.
33. Jares-Erijman, E. A., and Jovin, T. M. (2006) Imaging molecular interactions in living cells by FRET microscopy. *Curr. Opin. Chem. Biol. 10*, 409–416.

BI8009482